

Differential Phase Interferometry with the Keck Telescopes

G. Vasisht^a, M. M. Colavita^a

^aJet Propulsion Laboratory, California Institute of Technology

ABSTRACT

We summarize the Differential Phase (DP) technique as well as the planned implementation at the Keck Interferometer. Multicolor phase measurements are potentially a powerful astrophysical probe – and can allow ground-based direct detection of extrasolar planets. Better than 0.1 mrad phase measurements in the infrared can allow the Keck Interferometer to detect radiation from the so-called hot-Jupiter or “Roaster” class of planets. At JPL, we are presently developing and testing instrumentation that will enable these extremely sensitive measurements. First on-sky observations are expected to start in mid-2004. In this article we describe DP and other related techniques, provide an outline of the instrument and present results from preliminary laboratory experiments.

Keywords: Stellar Interferometer, fringe tracking, group-delay tracking, Keck Interferometer, infrared detectors, differential phase

1. INTRODUCTION

Direct detection of extrasolar planets with ground based instruments (which implies detection of the planet’s irradiance, as opposed to indirect detection e.g. via gravitational deflection) is a difficult problem primarily due to the large flux ratio between the parent star and the planet. The planet versus star flux ratio of a Jupiter mass planet orbiting at 0.1 AU from a G-type main sequence star is $\simeq 10^{-7}$ in the visible, and $\simeq 10^{-4}$ at 5 microns (e.g. Burrows et al. 2001). The equilibrium surface temperature of such a planet is about 10^3 K – hence the moniker “hot-Jupiter” or “Roaster” for these planets. At a distance of 25 pc, the angular separation between a Roaster and its star is about 5 milli-arcseconds i.e. an order of magnitude less than the diffraction limit of the largest ground based telescopes in the near infrared, including the 10 m diameter Kecks. However, an interferometric technique called Differential Phase (DP) can provide the necessary measurements for direct detection of Roasters and even help characterize their atmospheres (see Akesson et al. 2000).

2. DIFFERENTIAL PHASE AND RELATED TECHNIQUES

2.1. Differential Phase

We first present the 2-color differential phase in somewhat simplistic terms. Given a judicious choice of colors, the phase response of an interferometer to a star with a faint orbiting planet, is a strong function of the measurement wavelength λ_i . The star-Roaster flux ratio $r(\lambda_i)$ results in systematic shift of the binary’s photocenter a distance $d_i = r(\lambda_i)A$, where A is the separation between the star and the planet projected onto the sky. The interferometer’s complex response can then be written as,

$$\Gamma_{\lambda_i} = V_i \exp(j\Phi_i), \quad (2.1)$$

where the phase as a function of wavelength is just,

$$\Phi_i = \phi_i^{atm} + \frac{k_i d_i B_p}{D}. \quad (2.2)$$

Further author information: (Send correspondence to G. Vasisht)
G. Vasisht: E-mail: gv@s383.jpl.nasa.gov, Telephone: 1 818 354 6979, MS 171-113, JPL, 4800 Oak Grove Dr., Pasadena CA 91109.

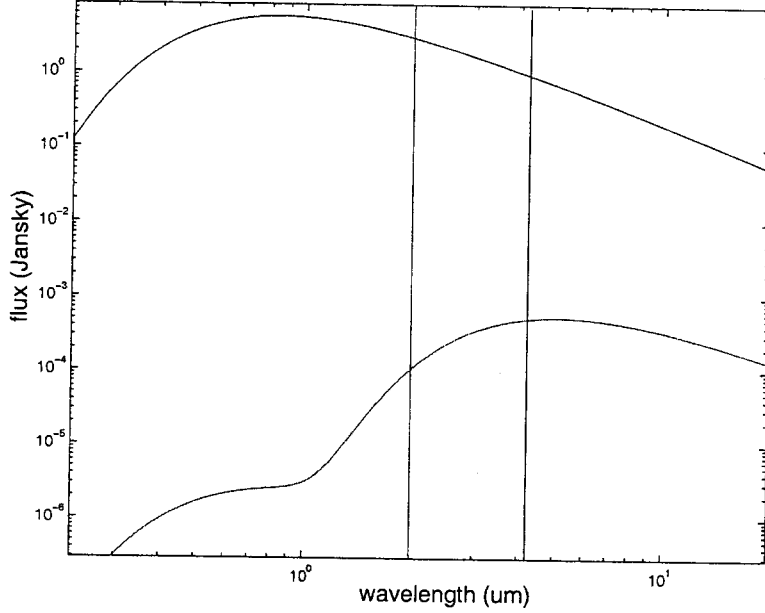


Figure 1. Relative fluxes from a Star-Roaster system. Star and planet are assumed to be blackbodies; $T_s = 5.9 \times 10^3$ K, $T_p = 1 \times 10^3$ K. The planet flux is the composite of both its intrinsic blackbody radiation as well as reflected starlight. The vertical lines bracket the DP wavelength range intended at Keck.

Here, $k_i = 2\pi/\lambda_i$ is the wave number, B_p is the projected interferometric baseline, D is the distance to the star and ϕ_i^{atm} is a residual atmospheric term that results from atmospheric turbulence driven by temperature fluctuations (of order 10's of microns). The relevant astrophysical signature can then be derived as a two-color phase difference (or DP),

$$\Delta s_{12} = \frac{\Phi_1}{k_1} - \frac{\Phi_2}{k_2} = \frac{AB_p}{D}(\tau_1 - \tau_2). \quad (2.3)$$

With a proper choice of colors (e.g. $\tau_1 \gg \tau_2$) the planetary signature at a single color may be extracted. In writing Eqn 2.3 we assume that the atmospheric term falls out – this is applicable for observations through a dry atmosphere at an excellent observing site, and of course for space based observations. The dry atmosphere is not very dispersive. An estimate of the magnitude of the astrophysical signature, based upon the example illustrated in figure 1, between 2 and 4 microns (i.e. the atmospheric K and L bands) is,

$$s = 100 \text{ pm} \left(\frac{B_p}{10^2 \text{ m}} \right) \left(\frac{A}{0.1 \text{ AU}} \right) \left(\frac{D}{20 \text{ pc}} \right)^{-1}.$$

Clearly, the size of the signature varies with Earth rotation (or projected baseline), the orbital inclination of the star-planet system, and in the case of non-zero inclination, the orbital phase of the planet.

In reality things are a quite a bit more complicated. In cases where the atmospheric leakage term becomes important, two colors no longer suffice and measurements must be performed at three or more colors. It was also realized via observations at the Palomar Testbed Interferometer (PTI) that the atmosphere is much more strongly dispersive than originally thought (Akeson et al. 2000). Large unexplained systematic residuals were found in PTI data. It was soon realized that these were due to water vapor turbulence. The residual phase leakage due to the atmosphere (Eqn 2.2) can then be written as

$$\phi_{atm} = \phi_{dry} + \phi_{wv},$$

where the latter term is due to water. A proper model of the water vapor refractive index across the major infrared bands supports the conjecture that water vapor was at least 20 times more dispersive than originally

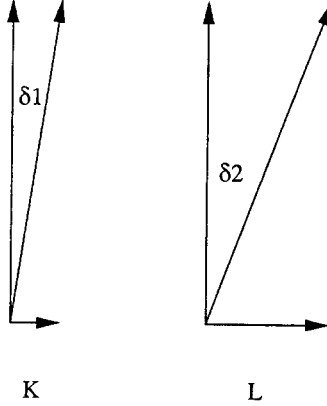


Figure 2. An illustration of DP with fringe phasors. The components due to the star and planet are drawn along the Y and X axes, respectively. The short observing wavelength K is to the left, while L is to the right. The observable is $\delta_2 - \delta_1$. Amplitudes of planet phasors are grossly exaggerated. The stellar component is equally bright at K & L, while the planet is fainter at K.

thought; this latter from extrapolations from optical effects of water vapor. It can be shown that for a good night on Mauna Kea, a high altitude and relatively dry site, the water vapor seeing component in the differential phase is about 10^3 times (30 nm rms) larger than the astrophysical signature. Given the pink statistics of water column fluctuations, these do not average very well; such fluctuation usually approximate Kolmogorov turbulence.

The most effective way to mitigate the effects of the wet atmosphere is to somehow estimate the fluctuations of the water columns above individual telescopes of the interferometer. One can use water vapor radiometry, however radiometers cannot measure spatial scales relevant to the interferometer. Another way is to simultaneously measure the differential phase on a nearby calibrator star (one that has no intrinsic DP signature i.e. an unresolved single star). There are two drawbacks to this technique: 1. It is hard to implement on an interferometer 2. Suitable targets are hard to find for most targets within the angular limitations set by water vapor anisoplanatism. A third way is to monitor the fluctuations of water absorption lines located within or outside astronomical bands. This can be accomplished by either photometry of the line, or fringe phase fluctuations within the line. Some of these resonances are unsaturated at Mauna Kea and small changes in the column result in relatively large changes in the fringe phase. Photometry of the line to the required accuracy is difficult due to scintillation effects. Probably the best approach is to take fringe measurements at several wavelengths and to use the different wavelength dependencies of water and the source differential phase to separate the atmospheric and astronomical terms. If the refractivities of all offending components of the atmosphere and estimates of the shape of the differential phase signature are known and none of these are degenerate – then the magnitude of all terms including the target’s astrophysical signature may be estimated from phase measurements at several wavelengths and subjecting the data to the usual least squares methods.

Finally, the small astrophysical signature requires rather precision measurements, with phase measurement noise $\sigma_\phi \simeq 10^{-5}$ mrad rms (about 10 pm); usually σ_ϕ is given S^{-1} rad. Here, S is the signal-to-noise ratio of an ideal fringe measurement; for an infrared background limited source S is given as

$$S^2 \simeq \frac{N^2 V^2}{B}, \quad (2.4)$$

where N is the photon rate from the source, and B is the sky and local background rate. With the large collecting power of the Kecks, and assuming our standard G-star and Roaster system at 20 pc, adequate signal-to-noise may be achieved in a few minutes of integration.

2.2. Related Techniques

Besides DP, there are a couple of related direct detection schemes. They have both advantages vis-a-vis drawbacks when compared to DP. We describe two here that have the advantage that to first order these are immune to atmospheric turbulence and related dispersion. First is differential closure phase, a method that requires three input apertures and is therefore not immediately applicable to the Keck Interferometer.

Let ϕ_{ij}^ν be the phase across baseline b_{ij} of a three element interferometer ($i, j = 1, 2, 3$) at color ν . We drop the color index ν temporarily. Then

$$\phi_{ij} = \psi_i - \psi_j + \Phi_{ij}, \quad (2.5)$$

where ψ_i is the total phase accumulation at aperture i due to propagation through the atmospheric column, telescope and beamtrains. Φ_{ij} is the astrophysical phase on that baseline, where once again the response is written as $\Gamma_{ij} = V_{ij} \exp(-i\Phi_{ij})$. The closure phase or bispectrum is given by,

$$\Phi_{ijk} = \phi_{ij} + \phi_{jk} + \phi_{ki} \rightarrow \Phi_{ij} + \Phi_{jk} + \Phi_{ki}$$

using circulating indices and leads to the usual cancellation of telescope based errors. A 2-color bispectrum which also immune to certain baseline dependent errors, is then constructed as -

$$\Theta_{ijk}^{\mu\nu} \equiv \Phi_{ijk}^\mu - \Phi_{ijk}^\nu. \quad (2.7)$$

The 2-color bispectrum is immune to dispersion induced systematics. Sources of systematic error are slow drifts in the instrumental bispectrum - however since this quantity is monitored simultaneously at two colors, one can solve easily for instrumental and astrophysical terms.

The bispectrum is a noisier quantity than the Michelson fringe phase. The square of the SNR in the Michelson case is given in Eqn 2.4 assuming that shot noise due to the thermal background dominates, i.e $B > N$. For the 2-color bispectra the squared-SNR per baseline is given by

$$S_C^2 \simeq \frac{N^2 V_{ij}^2}{2B}$$

and is lower as a result of additional beam-splitting in a 3-way combiner. Since the closure phase is determined by adding three equally noisy phasors, the differential bispectrum is a factor $\sqrt{6}$ noisier.

Another variant is direct detection of planets by precision measurement visibilities; visibility is the amplitude V of the interferometer's response in Eqn 2.1. Optical and infrared interferometers usually measure the visibility amplitude (e.g. Colavita 1999) squared, V^2 , as its estimator is unbiased. For a binary system, the V^2 can be expressed in terms of the visibilities of the two components of binary and their flux ratio r as,

$$V^2 = \frac{V_1^2 + r^2 V_2^2 + 2r V_1 V_2 \cos(k B_p \theta)}{(1+r)^2}. \quad (2.8)$$

The angle $\theta = A/D$ is just the angular separation of the binary. Whence each component is unresolved by the interferometer and the flux ratio is small, i.e. $V_1 = V_2 \simeq 1$ and $r \ll 1$, it is easily shown that V^2 evolves between the extrema 1 and $1-2r$, with changes in the projected baseline and orbital phase. In order to detect the planet, the visibility must be measured to better than 1 part in 10^4 . This is not easily done. Fringe phase estimates are zero-mean and inherently less noisy than V^2 estimates ($\sigma_\phi^2 \propto (N+B)/N^2$ versus $\sigma_{V^2}^2 \propto (N^2+B^2)/N^4$, with $B > N$ in the background limit). However, a distinct advantage of the V^2 estimator is that it is *immune* to water vapor turbulence.

Single mode fiber optic beam combiners, with photometric taps, have allowed visibility measurements to 0.3% (Perrin 1999). It may be possible to obtain greater accuracies in a differential scheme. The observable would be the ratio of visibilities measured at the short (K) and long (L) wavelengths; the latter will vary depending on orientation of the star-planet system. With concurrent photometric monitoring, a single mode fiber combiner is nominally immune to spatial distortions that affect visibility, but provides little immunity against temporal blurring. Temporal blurring can be reduced by sampling the fringe at rates significantly faster (times 10) than the coherence time.



Figure 3. The twin Keck Telescopes on Mauna Kea viewed from the South.

3. DIFFERENTIAL PHASE AT KECK

The Keck Interferometer combines the two 10-m diameter Keck telescopes for high sensitivity infrared (in atmospheric transmission bands between 1.5 and 14 microns) fringe measurements (Colavita & Wizinowich 2002). First fringes on the 85-m baseline between Keck I and Keck II were obtained in March 2001, with both telescopes using their adaptive optics (AO) systems. Subsequent work has focussed on engineering aspects including system validation, improving sensitivity, increasing automation, and adding functionality in preparation of nulling and DP interferometry – as well as scientific observations in the classic V^2 mode.

The first DP verification observations are expected to begin in July 2004. At the time of writing this paper all DP activities, except for the installation of the vacuum delay-lines, are confined to the Keck laboratory at JPL. The laboratory testbed setup at JPL includes all specialized hardware components developed for DP, along with other usual components comprising a stellar interferometer such as delay lines and fringe trackers etc. The goal of the testbed is to demonstrate differential fringe phase measurements to the required 0.1 mrad levels using a pseudo-star.

3.1. Major Components of the Interferometer

The differential phase architecture will use multicolor fringe position measurements across K and L bands (2.0 - 4.2 microns). This instrument mode is enabled by several standard subsystems of the interferometer, summarized below, along with specialized instrumentation necessarily required for a precision fringe engine.

First of the major subsystems of the interferometer are the two Keck telescopes and their adaptive optics systems. These are natural guide star AOs. Each AO uses a Shack-Hartmann wavefront sensor, a fast readout CCD and a 349 actuator deformable mirror. The corrected wavefront is collimated and the infrared light is extracted with a dichroic beamsplitter and propagated along each of two arms as 112 mm diameter beam. Dual star modules are located adjacent to the AO systems on the Nasmyth platforms; for DP observations simple flats are used to relay the output beams from the AO to the telescope Coude train. The Coude train uses a series of four flats to relay the beam to the observatory basement level. The last of these four mirrors is attached to the telescope pier beneath the azimuth axis. Another set of reflections is then used to compensate for image rotation from where on the light is directed through Coude tunnels in the basement toward the beam combination laboratory. Gross mismatches in the optical path within the observatory are compensated by positioning long delay line carts. Sidereal delay is removed by positioning of a combination of vacuum delay lines and the cat's eye fast delay line carts. Vacuum delay lines can only be crudely positioned to mm levels, and therefore allow removal of sidereal delay to similar levels. Fine compensation of the delay, necessary for fringe finding and measurements, is then done via the fast delay lines – these can track a commanded position to few

nanometer accuracies. The output of the fast delay lines is compressed by 4:1 beam compressing telescopes to a diameter of 26 mm. This compressed beam is delivered to the vacuum delay lines, which provide ± 63 m of delay path, adequate for observing objects located up to 52 degrees from zenith.

The output of the vacuum delay lines is then delivered to the beam combining optics and the fringe measuring engine. These are further discussed below. A heterodyne metrology laser is launched from the beam combination area and monitors the differential internal path at rapid rates (4 kHz). The fast delay lines servo to this signal, which mitigates pathlength jitter from observatory generated (mechanical) vibrations. The metrology, however, cannot easily measure pathlengths within the telescopes. For these a bank of accelerometers measures the dynamics of the primary, secondary, and tertiary mirrors. The resultant pathlength information is fed forward to the fast delay lines.

3.2. Components Developed for Differential Phase

Enabling the DP mode requires the aforementioned specialized hardware that we now describe further. First are the vacuum delay lines (VDLs), needed for quasi-static longitudinal dispersion control. Since an air delay line results in the sidereal delay being compensated for in air, large amounts of dispersion results between the K and L bands even at modest zenith angles. Use of a vacuum delay line obviates the need for atmospheric dispersion controllers, and related calibration issues; it limits dispersion to turbulence generated differential columns. Each VDL cart rides on two round precision rails mounted inside a vacuum chamber that consists of 11 separate stainless steel flanged sections each 3.3 meters long. The rails rest in saddles, while the saddles rest on adjustment screws inside the take. The VDL cart consists of a large corner-cube mounted on one of two inverted pendulum structures with offset resonance frequencies (in the 1 Hz range). The pendulums are coupled via a short-circuited voice coil that provides passive damping. The VDL cart is driven by a tractor cart via a flexible link (and a vacuum compatible micro-stepper motor). The positioning of the cart and optic is by means of a local heterodyne laser metrology gauge.

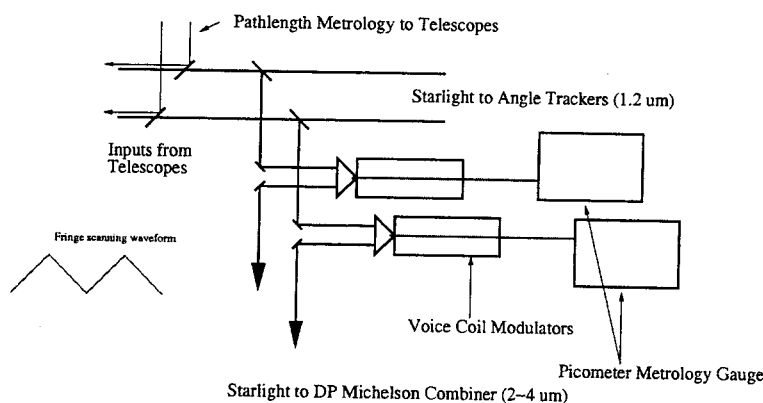


Figure 4. A Schematic Layout of DP Modulation. Starlight from the two telescopes enters at the left and is split into KL light from interferometry and J light for angle tracking. The two modulators execute precision pathlength modulation that is monitored with a pico-metrology system. The modulated beams are relayed to a Michelson combiner, not shown in the figure below.

After traversing the continuous motion fast delay-line carts, the beams are further compressed to 26 mm, and relayed to the VDLs. Beams delayed by the VDL carts then enter the optical switchyard located in the beam combining laboratory. All instrument feeds are invariably implemented as shortpass dichroics. Feed dichroics reflect K & L bands into a Michelson beam combiner, while transmitting J band and leaking some visible light further downstream for angle tracking and beamtrain alignment, respectively.

The combiner breadboard features a stimulus or artificial star kinematically mounted on a smaller mezzanine breadboard. The stimulus can generate a single-mode collimated white light beam, injected into the

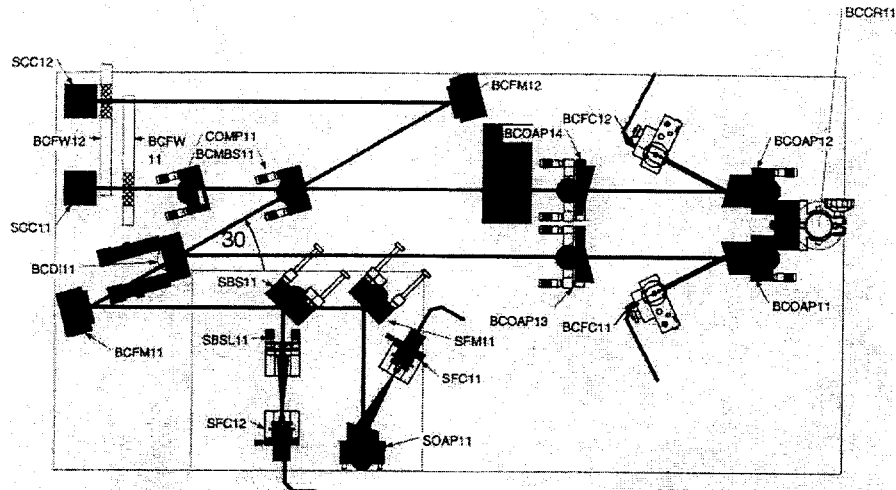


Figure 5. A Schematic Layout of the DP Michelson Combiner. Starlight is directed into the combiner at inputs SCC11 and SCC12, and is combined at the main beamsplitter BCMB11. The combined light from the two Kecks is coupled into single mode infrared fibers at BCFC11 and BCFC12.

interferometer via a leaky dichroic and propagated upstream (SFC11 in figure 3). Corner cubes placed in the parent beamtrains at any point upstream allow the interferometer to be operated in internal FTS mode for calibrations, or for engineering monitoring of the beamtrain. The stimulus also houses a solid state boresight laser (660 nm; SFC12), and has provisions for injection of a He-Ne “constant term” (CT) metrology signal for monitoring AC fluctuations of the internal OPD.

Within the combiner, beam combination takes place at the main beamsplitter MBS11 (fig. 5) which has nearly 50-50 performance over the 1.9-4.2 μm science band, and a 30-70 performance in the laser band around 630 nm. The compensator COMP11 is matched in thickness to MBS11 to control dispersion between K and L bands to within 100 nm. Combined beams from complementary sides of the beamsplitter are coupled into fluoride-glass SM fibers with optimized off-axis parabolas (e.g. OAP12). The fibers act as spatial filters for the combined beam, translating dynamic wavefront and pointing errors into coupling variations and resultant output intensity scintillation. The fibers are ≈ 2.0 m in length and terminate at beam launch points within the camera cryostat (called Fatcat-III), via a flange mounted vacuum feedthrough. The fibers also limit extraneous thermal background to a single spatial mode – in addition, the warm end of each fiber illuminates an annular off-axis parabola (OAP13 or OAP14) which terminates on the emissive cold surface of a three-stage solid-state refrigerator mounted on post BCCR11, forming a pseudo Lyot stop.

Within the cryostats, each fiber output is re-collimated to 20 mm with an achromatic doublet and propagated along one of four identical optical relays. The beams are bandpass filtered with filters selectable from five locations on a filter wheel driven by an external dc servo motor with a precision gearbox and optical encoders. The same mechanism is used for accurate positioning of prisms into the beam path. Beams may be dispersed with low ($R \sim 10^2$) dispersion direct view prisms, corresponding to $\approx 10 - 36$ pixel wide spectra on the detector.

The Fatcat cryostat uses liquid nitrogen as coolant. It is a bi-vessel dewar with the inner vessel supporting both the detector and optical tree, with 95 % of the thermal load on the outer vessel. The inner vessel may be pumped-on to solidify the nitrogen for lower (60 K) temperature operation, which improves the detector dark current. Closed cycle refrigerators were not considered out of the concern that a pistoning cold head would subject the sensitive optical system to intolerable levels of microdynamics. With passive cooling, long term pointing drifts are observed to be less than 10^{-3} pixels hr^{-1} , critical for limiting wavelength drifts between spectrometer calibrations since very precise wavelengths are necessary for DP; also the fiber feeds allow isolation from drifts in external alignment. In addition, with a first mechanical resonance well above 100 Hz, the aluminum mounting

tree in the dewars makes the sensitive optical system relatively immune to external vibrational excitations.

Last but not the least is the need for an ultra-precision fringe engine. It is hard to build a perfectly linear and stable fringe engine, but one can build one with a close to linear phase response and one can constantly monitor the non-linearities and temporal changes in this response. Since we measure the Michelson fringe phaser by pathlength modulation it is important that the measuring engine introduce no systematic errors in the phase estimators. The fringe modulator design is absolutely crucial. This is implemented as a corner-cube (modulation is performed in collimated space) on a reactionless voice coil stage. The stage is driven in a 250 Hz triangle wave that is approximated with the first three Fourier components of a triangle; these are predistorted to account for the complex response of the drive amplifiers and electronics. Fringe measurements are executed in the most linear up-and-down regions of the ramp. Since modulator non-linearities and drifts cannot be entirely eliminated we have chosen to monitor the modulation with a separate laser metrology system with 10's of picometer short term accuracy (Gursel 2002). The modulator and metrology, in conjunction with the detector and fringe demodulator form the basis for a stable fringe engine.

3.3. Fringe Measurement and Tracking

Fatcat measures the fringe at twice the rate of modulation (500 Hz); one measurement each for the up-stroke and the down-stroke. Position estimates are computed and used in real-time to servo the FDL against pathlength motion due to the atmosphere (Vasisht et al. 2003). Since the atmospheric coherence time is about 10 ms at K band, a 2 ms sample rate is adequate. Raw fringe data are also telemetered to a data archive for DP post processing.

Both the Fatcat camera read and compute cycle and fringe modulation are synchronized through timing generation and distribution electronics that are referenced to a 1 PPS signal derived from UTC. The camera is clocked at the fundamental frame rate, and the triangle modulation at the same same rate is implemented on a voice-coil modulator on one arm of the interferometer; each is nominally 250 Hz as described before, but have soft adjusts. The stroke amplitude is set to be slightly larger than the longest observable wavelength, in this case 4.2 microns. The camera acquires eight equally spaced reads of the modulated fringe on all pixels, along with detector reset pedestals. Complex fringe phasors are derived from the raw camera reads, for all pixels, after subtraction of dark pixel biases. Phasors are dewarped to correct for channel wavelength to stroke length mismatch, and can be rotated to account for any static dispersion in the internal path. All derived quantities, such as fringe phase and visibility, and instantaneous SNR and photon rate, are computed at the frame rate.

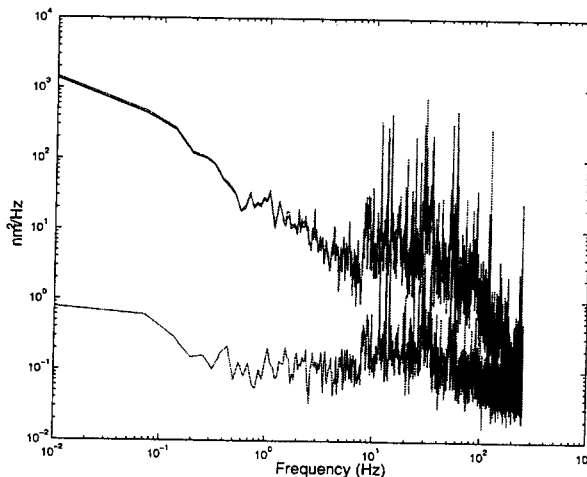


Figure 6. Results of internal DP tests at Keck. PSDs of optical path of two channels (2.0 and 2.35 microns; K band) are the top two traces. The bottom trace shows the differential of these channels, white to a few seconds. The rms in this example is about 300 pm in 1 sec. The low frequency power could be due to internal humidity.

Given their coherence length the multi-color fringe packets usually have several fringe cycles with adequate SNR for white light tracking. However, for accurate DP estimation it becomes necessary to track on the central fringe – or equivalently at zero group delay. The group delay is estimated real-time with the complex spectrometer phasors, with a Discrete Fourier transform (DFT) followed by peak detection. In order to finesse the estimate from the crude DFT, power is recomputed at half integral bins around the peak and a parabolic fit is applied. At low photon rates, the noisy group delay estimate may lack adequate SNR. For improved SNR, the noisy spectrometer phasors are phase referenced (rotated) to the instantaneous white light phases and averaged for several samples. Group delay estimates are used, in conjunction with the white-light tracker error (this ranges between $-\pi$ and π), to shift the tracking center of the white light (WL) tracker to the central fringe. It is not always necessary to have a WL-tracker – for bright stars with adequate SNR for group delay estimation, the instrument can be set up for pure group delay tracking.

3.4. Instrumental Error Sources

Two major systematic error sources at the level of the interferometer are easily identified and have to be calibrated for during an observing sequence; a sample observing sequence may alternate between the target and calibrator stars as: star – calibrator 1 – star — calibrator 2 etc. with a 10 minute chop time. Up to four calibrators in angular proximity to the target star may be chosen.

The first important systematic error that affects the differential phase metric results from angular dispersion due to atmospheric refraction; the angle of arrival difference is of order 0.05 arcsec between K and L bands. Due to the large pupil compression (a factor 400 between the telescope diameter and the final 26 mm beam) and long internal paths, $\simeq 200$ m, the K and L pupils are sheared. The shear changes with zenith angle leads to a differential beamwalk between the K and L band pupils, resulting in phase errors (due to optical figure errors) as large as 50 pm per degree of zenith angle at ZA = 30 degrees. Calibration will involve observing nearby compact stars with small ZA separations such that beamwalk effects may be described by a linear model; the beamwalk for the target may then be derived by interpolation.

Another important error source is diffraction. As a result of the small beam diameter (26 mm diameter) and up to ± 60 m of internal path difference, diffraction results in chromatic pathlength differences that evolve with stellar delay. The Fresnel number varies between 10 and 5 for 2-4 microns for about 30 m of propagation path.

Finally, there are the effects of systematic drifts in the detector gains and biases. For instance systematic drifts in detector biases of magnitude 1 part in 10^5 of the stellar photon rate, within a 10 minute detector calibration cycle, bias the measured phase. In our experience, with proper clocking and temperature control of the Rockwell HgCdTe arrays, this problem is circumvented.

4. CONCLUSIONS

We have described how ultra-precision Differential Phase measurements can possibly detect the planetary signatures of Extrasolar Giant Planets. Fluctuations in the columns of “parasitic” atmospheric components such as water make these observations challenging. We also described two alternative methodologies that are in principle immune to these fluctuations, but have complications of their own. At the Keck Interferometer, we are working towards making differential phase an observing mode by implementing vacuum delay lines to control sidereal longitudinal dispersion alongwith a precision fringe engine to measure phases with unprecedented accuracy across the 2-4 micron wavelength range.

GV acknowledges the contributions of fellow colleagues at JPL: M. M. Colavita, J. Moore, Y. Gursel, R. Ligon, M. Shao, M. Swain and R. L. Akeson. This work was performed at the Jet Propulsion Laboratory, California Institute of Technology, under contract with the National Aeronautics and Space Administration.

ACKNOWLEDGMENTS

GV acknowledges the contributions of fellow colleagues at JPL: M. M. Colavita, J. Moore, Y. Gursel, R. Ligon, M. Shao, M. Swain and R. L. Akeson. This work was performed at the Jet Propulsion Laboratory, California Institute of Technology, under contract with the National Aeronautics and Space Administration.

REFERENCES

1. R.L. Akeson, M.R. Swain, and M.M. Colavita "Differential Phase Technique with the Keck Interferometer," *Proc. SPIE*, **4006**, 321 (2000).
2. A.S. Burrows, W.B. Hubbard, J.I. Lunine, and J. Liebert "The Theory of Brown Dwarfs and Extrasolar Giant Planets," *Rev. Mod. Phys.*, **73**, 719 (2001).
3. M.M. Colavita, and P.L. Wizinowich "The Keck Interferometer," *Proc. SPIE*, **4838**, 79 (2002).
4. M.M. Colavita "Visibility Calibration with the Palomar Testbed Interferometer" *Proc. Astro. Soc. Pac.*, **111**, 111 (1999).
5. G. Perrin "The Calibration of Interferometric Visibilities Obtained with Single Mode Optical Interferometers," *Astr. Phys. Jrrnl.*, **510**, 505 (1999).
6. G. Vasisht, A. Booth, M.M. Colavita, R.L. Johnson, E.R. Ligon, J.D. Moore, and D.L. Palmer "Performance and Verification of Keck Fringe Detection and Tracking System," *Proc. SPIE*, **4838**, 824, 2003.
7. Y. Gursel, "Picometer-accuracy Laser-metrology Gauge for the Keck Interferometer Differential Phase Subsystem," *SPIE*, **4838**, 995, 2003.